

**HHS PUBLIC ACCESS**

Author manuscript

IEEE Trans Ultrason Ferroelectr Freq Control. Author manuscript; available in PMC 2017 February 01.

Published in final edited form as:

IEEE Trans Ultrason Ferroelectr Freq Control. 2016 February ; 63(2): 266–274. doi:10.1109/TUFFC.2015.2506000.**Design, Fabrication and Characterization of A Bi-Frequency Co-Linear Array****Zhuochen Wang,**

Department of Mechanical and Aerospace Engineering, North Carolina State University, Raleigh, NC 27695, USA

Sibo Li,

Department of Mechanical and Aerospace Engineering, North Carolina State University, Raleigh, NC 27695, USA

Tomasz J Czernuszewicz,

Joint Department of Biomedical Engineering, University of North Carolina and NC State University, Chapel Hill, NC 27599, USA

Caterina M. Gallippi,

Joint Department of Biomedical Engineering, University of North Carolina and NC State University, Chapel Hill, NC 27599, USA

Ruibin Liu,

Blatek, Inc., State College, PA 16801, USA

Xuecang Geng, and

Blatek, Inc., State College, PA 16801, USA

Xiaoning Jiang [Member, IEEE]

Department of Mechanical and Aerospace Engineering, North Carolina State University, Raleigh, NC 27695, USA

Abstract

Ultrasound imaging with high resolution and large penetration depth has been increasingly adopted in medical diagnosis, surgery guidance, and treatment assessment. Conventional ultrasound works at a particular frequency, with a -6 dB fractional bandwidth of $\sim 70\%$, limiting the imaging resolution or depth of field. In this paper, a bi-frequency co-linear array with resonant frequencies of 8 MHz and 20 MHz was investigated to meet the requirements of resolution and penetration depth for a broad range of ultrasound imaging applications. Specifically, a 32-element bi-frequency co-linear array was designed and fabricated, followed by element characterization and real-time sectorial scan (S-scan) phantom imaging using a Verasonics system. The bi-frequency co-linear array was tested in four different modes by switching between low and high frequencies on transmit and receive. The four modes included the following: (1) transmit low, receive low, (2) transmit low, receive high, (3) transmit high, receive low, (4) transmit high,

receive high. After testing, the axial and lateral resolutions of all modes were calculated and compared. The results of this study suggest that bi-frequency co-linear arrays are potential aids for wideband fundamental imaging and harmonic/sub-harmonic imaging.

Keywords

bi-frequency ultrasound; composite transducer; co-linear array

I. Introduction

In conventional ultrasonography, tradeoffs exist between imaging resolution and penetration depth [1, 2]. Imaging with low frequency ultrasound can result in images with large penetration depths, but with low resolutions, while imaging with high frequency ultrasound offers higher spatial resolutions and shallower penetration depths. Therefore, transducers or arrays with wide bandwidths, for example from 5 MHz to 20 MHz, are highly desirable for the diagnostic medical imaging of different targets [3 - 10] in regards to optimal imaging resolution and penetration depth.

In addition to standard fundamental B-mode imaging, a broadband transducer is useful in harmonic imaging and sub-harmonic imaging. Harmonic imaging modes are desirable because they show less near-field and side lobe artifact, and have better signal-to-noise ratio (SNR), cleaner images, and overall, higher resolutions [11]. Moreover, harmonic imaging can be used in conjunction with ultrasound contrast agents (UCA) to improve the visualization and assessment of cardiac cavities, large vessels, and tissue vascularity. Sub-harmonic imaging in particular has been shown to achieve very high agent-to-tissue ratios because the contribution of tissue is minimal at acoustic pressures currently used in diagnostic ultrasound [12].

In order to achieve the advanced ultrasound imaging mentioned above, numerous studies on broadband transducers and arrays have been conducted. The usage of piezoelectric composite materials is an effective method to increase the bandwidth of a piezoelectric ultrasound transducer. 1-3 piezoelectric composite materials have favorable merits including high electromechanical coupling coefficients for broad bandwidth, low acoustic impedance for better acoustic matching, and relatively easy formation of complex shapes [13 - 16]. Compared to solid ceramic transducers, 1-3 piezoelectric composite transducers have been shown to dramatically increase the fractional bandwidth [17 - 20], although the fabrication of composites is more complicated.

Another approach to achieve a broadband transducer or multi-frequency application is to adopt a multi-layer transducer structure. A number of dual-layer transducers have been developed to achieve imaging at multiple frequencies. De Fraguier *et al.* designed a bi-frequency transducer with only one active layer, which functioned in both half wavelength mode and quarter wavelength mode by tuning the impedance of the backing layer [21]. This bi-frequency transducer worked at 2.4 MHz for Doppler imaging in quarter wavelength mode and 4.6 MHz for B-mode imaging in half wavelength mode. Saitoh *et al.* reported a dual frequency ultrasound probe that could be used to obtain Doppler imaging (3.75 MHz)

and B-mode imaging (7.5 MHz) simultaneously [22]. This probe included two PZT layers with thicknesses of 270 μm and 190 μm , respectively, which were poled in opposite direction and bonded together to form the multi-frequency transducer. Similarly, Hossack *et al.* developed a 2 MHz/4 MHz dual-layer ultrasound transducer for harmonic imaging [23]. In Hossack's design, two 1-3 piezoelectric composite layers with the same thicknesses of 440 μm and the same poling directions were bonded together. The two layers were then activated together to transmit at the fundamental frequency (2 MHz), while the top layer alone was used as the receiver of the second harmonic echo (4 MHz). Our group previously presented a prototype of a 2-element dual-layer bi-frequency transducer, which achieved a wide bandwidth, ranging from 5 MHz to 20 MHz [24]. This dual-frequency transducer consisted of two layers of PZT-5H piezoelectric 1-3 composites with the same aperture sizes and thicknesses of 100 μm . The transducer was designed to operate in two different modes: (1) a high frequency mode, where only the top piezoelectric layer was the active layer, and (2) a low frequency mode, where both piezoelectric layers were activated electrically in parallel to achieve a lower frequency.

In this paper, the design, fabrication, testing, and imaging experiments of a new 32-element bi-frequency co-linear array are reported. This array was designed to operate at two frequencies to achieve a broadband response, which can be applied in a range of biomedical ultrasound imaging applications. The array was fabricated using PZT-5H piezoelectric 1-3 composite, followed by electrical and acoustic characterizations. Real-time phantom imaging was accomplished with a Verasonics Vantage system (Verasonics, Redmond, WA). In order to study the feasibility of fundamental, harmonic, and sub-harmonic imaging with this array, four different working modes, including: (1) transmit low, receive low (L/L mode), (2) transmit low, receive high (L/H mode), (3) transmit high, receive low (H/L mode), and (4) transmit high, receive high (H/H mode), were investigated and compared. Spatial resolutions of each working mode were estimated by using a wire target response method [25, 26].

II. Methods

A. Structure Design

The co-linear array was designed with a dual-layer structure and two center frequencies of 7.5 MHz and 15 MHz, respectively (Figure 1a). To achieve "high frequency" (HF) mode, the top piezoelectric layer was activated alone, so that a high frequency wave could be transmitted or received (Figure 1b). To achieve "low frequency" (LF) mode, the top layer and bottom layer of each element were electrically activated in parallel by applying a signal between the ground and the shorted top/bottom layers of each element to obtain a lower frequency wave (Figure 1c). Further details of the wire connections are reported in our previous work [24]. This co-linear array works in four different modes: a) L/L mode, where both transmitting and receiving are conducted with both layers at the low frequency; b) H/H mode, where both transmitting and receiving are conducted with only the top layer at the high frequency; c) L/H mode, where the wave is transmitted with both layers at the low frequency and the echo is received with the top layer at the high frequency; and d) H/L

mode, where the wave is transmitted with the top layer at the high frequency and the echo is received with both layers at the low frequency.

In the dual-layer transducer design, the two active layers cannot be bonded together directly. Otherwise alias echoes will be generated, which can shift the resonant frequencies of both layers and impact the bandwidth [27]. Therefore, a frequency-selective isolation layer with a low acoustic impedance, implemented as a quarter wavelength anti-matching layer of the selected frequency, was placed in between the two piezoelectric layers, in order to isolate the top layer from the bottom layer in the HF mode [28]. This isolation layer did not significantly affect the LF mode because the isolation layer was thin compared to the wavelength of the LF mode [29]. The isolation layer thickness and the material selection, as well as the pulse-echo responses of both frequency modes, were designed using the KLM model [30]. The isolation layer was achieved by controlling the bonding layer thickness, and it was used to bond the two piezoelectric layers together [31]. In order to increase the bandwidth, a PZT-5H piezoelectric 1-3 composite was used in the configuration. The acoustic field, with beam focusing and steering for both frequencies, was simulated by using the Field II program [32, 33]. Further details of the design and simulation can be found in our previous work [34, 35].

B. Transducer Fabrication

A PZT-5H/epoxy (Epo-tek 301, Epoxy Technology, US) 1-3 composite with a ceramic volume fraction (CVF) of 64% was used as active material in the transducer. To construct the 1-3 composite, a dice-and-fill process was used. Once the composite pieces were lapped to the designed thickness, both sides were deposited with a layer of Ti/Au (10nm/100nm).

Two 100 μm PZT-5H piezoelectric 1-3 composite layers with gold sputtered on both sides were prepared first. The top surface was then diced to form the electrode pattern. To achieve the dual-layer structure, two active layers were bonded together back to back, and two flex circuits were used for the interconnect assembly. After being bonded with the matching layer and the flex circuits, the assembly was encased in a plastic housing and filled with backing material. Printed circuit board (PCB) with a commercial connector (53748-0408, Molex Inc., Lisle, IL) was used for cable wiring between the flex circuits and the standard connector (DL260, ITT Corporation, Santa Ana, CA) of the Verasonics system.

C. Transducer Characterization

The co-linear array was characterized by measuring the capacitance of each element, pulse-echo responses, and beam focusing/steering profiles. Capacitance and dielectric loss of each element were measured using an impedance analyzer (Agilent 4294A, Agilent Technologies, Santa Clara, CA). Center frequency and loop sensitivity were obtained by measuring the pulse-echo response of the array elements using a Pulser/Receiver (Olympus 5077 PR, Olympus Corp, Newton, MA) and an oscilloscope (Agilent DSO7014B, Agilent Technologies, Santa Clara, CA). The voltage of the applied pulse was set to be 100 V during the pulse-echo test. A steel block was placed in front of the co-linear array at a distance of 5 mm to serve as a reflection target in a water tank.

Beam focusing and steering were tested with a Verasonics Vantage system, a hydrophone (HGL-0200, ONDA, Co., Sunnyvale, CA), and the Labview program (National Instruments Corporation, Austin, TX). Both the LF and the HF transmitting modes were tested, with the HF set at 15.6 MHz and the LF set at 7.8 MHz, based on the frequency settings available on the Verasonics system. The scanning area was programmed to be 27 mm by 20 mm, with a step of 0.25 mm in both the axial and lateral directions. For display, beam plots were upsampled by a factor of 10 using spline interpolation.

D. Phantom Imaging

Phantom imaging using the prototyped 32-element co-linear array was conducted with the Verasonics system. B-mode images were rendered using the proprietary Verasonics beamforming algorithm, and the raw RF data was saved to the hard drive of the computer.

A multi-purpose multi-tissue ultrasound phantom (Model 040, CIRS Inc., Norfolk, Virginia, USA) was used as the target to evaluate the axial and lateral resolution of the co-linear array transducer. This is a tissue-equivalent test object with an attenuation coefficient of 0.5 dB/cm•MHz. The wire targets consisted of six pairs of 0.1 mm diameter parallel wires. Each pair of wires was spaced vertically by 0.5, 1, 2, 3, 4 and 5 mm intervals (± 0.2 mm) at a depth of 25 mm from the transducer surface (Figure 2).

The 32 element bi-frequency co-linear array transducer that was connected to the Verasonics system was placed on top of the commercial phantom to obtain real-time S-scan imaging in a range of 0 to 30 mm in depth with a steering angle of 30°. A detachable scanning well was installed on the testing surface of the ultrasound phantom during the phantom imaging test. The detachable scanning well was filled with water for acoustic coupling between the co-linear array transducer and the test phantom.

All four operation modes, including the L/L mode, the H/H mode, the L/H mode, and the H/L mode, were tested in the phantom imaging experiment. First, the axial resolution of the different modes was qualitatively estimated from the B-mode imaging directly by observing the overlap between wire targets. Then, the axial and lateral resolutions were calculated quantitatively from the beam width of the wire target responses. The penetration depths of all four modes were studied by measuring the backscatter SNR in the phantom with a focal depth of 25 mm [36]. The "signal" was collected at 25.4 V excitation and the "noise" was collected at 1.6 V excitation, which is the lowest voltage supplied by the Verasonics system.

The Verasonics sampling frequency (quadruple of the base frequency) was set to be 62.5 MHz (15.6 MHz as base frequency), which is the maximum frequency setting of our Verasonics System. Due to the frequency limitation of the Verasonics System, the transmit frequencies were set at 15.6 MHz for the HF excitation and 7.8 MHz for the LF excitation (half of the HF mode), respectively. The focal depth was set to be 25 mm, the same depth as the wire targets. The driving voltage of each element was set to be 25.4 V with a 2-cycle burst excitation, which is considered the safest driving amplitude for the array.

III. Results

A. Transducer Design

Bandwidth—The frequencies of the different layers were designed to be 7.5 MHz and 15 MHz, respectively. In order to isolate the top layer from the bottom layer in the HF mode, a frequency-selective isolation layer, which also functions as a bonding layer, made of Epotek 301 (Epoxy Technology Inc, Billerica, MA) was used to bond the two piezoelectric layers. The thickness of the bonding layer was intended to be 10 μm by using the KLM model to achieve isolation while keeping a relatively low thickness. The aperture size of both active layers was 4 mm by 4 mm. The thickness of each piezoelectric layer was 100 μm . Dimensions and acoustic properties of the active and passive layers are shown in Table I.

Figure 3 shows the predicted pulse-echo response of the co-linear array transducer from KLM model simulations. For the LF mode, the center frequency was 9.54 MHz, and the -6 dB bandwidth ranged from 5.77 MHz to 13.3 MHz, resulting in a fractional bandwidth of 77.9%. For the HF mode, the center frequency was 15.7 MHz, and the -6 dB bandwidth ranged from 11.7 MHz to 19.8 MHz, a fractional bandwidth of 50.4%. These simulation results suggest that with this dual-layer design, a wide bandwidth in the range of 5 MHz to 20 MHz can be achieved.

Beamforming (simulation)—The pitch of the array for both top and bottom layers was 0.132 mm. The size in azimuth of each element was 0.112 mm and the size in elevation was 4 mm. Figure 4 shows the acoustic field simulation results for the LF and HF operation modes of the co-linear array. The focal depth was set to be 15 mm, and the beam profile for the LF mode is shown in Figure 4a, where no grating lobes are present. Figure 4b shows the LF beam profile at a 15° steering angle away from the axis, with the grating lobe amplitude of -65 dB lower than that of the main lobe. For the HF beamforming without steering, the grating lobes are less than -40 dB (Figure 4c). In the case of a 15° beam steering angle, the amplitude of the grating lobe is still at the level of -45 dB (Figure 4d). Further beam steering results are summarized in Table II. In most cases, the grating lobe is more than -20 dB lower than the main lobe, suggesting reasonable imaging performance with the designed pitch.

B. Characterization

A 32-element bi-frequency co-linear array transducer was prototyped at Blatek (Blatek Inc., State College, PA), as shown in Figure 5. Together with housing, the dimensions of the transducer were 18 mm \times 12 mm \times 10 mm. The flex circuits, PCB board, and additional wires were used for cable wiring between the elements and the Verasonics connector. Capacitance of each element, pulse-echo responses, and beam focusing/steering profiles were tested.

Capacitance measurement and pulse-echo responses—The mean (\pm standard deviation) capacitance of each element in the top layer was 165.41 pF \pm 8.38 pF, and dielectric loss was 0.018 \pm 0.003. The mean capacitance of elements in the bottom layer was

175.07 pF \pm 5.33 pF, and dielectric loss was 0.015 ± 0.0022 . Overall, the measured capacitance results supported the theoretical values for element capacitance (142 pF). Pulse-echo results of both the LF mode and the HF mode are shown in Figure 6a and 6b. The average center frequency in the LF mode was measured to be 7.9 MHz \pm 0.99 MHz. The average center frequency of the HF mode was measured to be 19.7 MHz \pm 0.56 MHz. The -6 dB fractional bandwidth of the LF mode was 55.8% and the -6 dB fractional bandwidth of the HF mode was 31.8%. The loop sensitivity of the LF and HF modes were calculated from the pulse-echo data as -31.6 dB \pm 2.61 dB and -35.7 dB \pm 1.8 dB, respectively.

The results given above demonstrate that the co-linear array was able to achieve two different resonant frequencies (7.9 MHz and 19.7 MHz), however the bandwidth was not as wide as expected. This discrepancy was most likely the result of improper isolation between the two layers. While the isolation layer was designed to be 10 μ m, the actual thickness of the isolation layer after production was only 2 μ m. Although imperfect, the isolation layer was functional to some degree; KLM simulation showed that the -6 dB bandwidth of the HF mode with a 2 μ m isolation layer was 30%, which supports the experimental result. A -6 dB bandwidth of the HF mode without an isolation layer was predicted to be only 24% (Figure 7).

Beamforming (experimental)—Beam focusing and steering were tested using the Verasonics system to apply a 2-cycle signal to each element with time delay and then using a hydrophone to measure acoustic pressure. In the LF transmitting mode, the transmit frequency was set to be 7.8 MHz; while the frequency of the HF mode was set to be 15.6 MHz. Figure 8a shows the beam profile of the LF transmitting mode. The -6 dB beam width when focusing at 15 mm was 0.725 mm. With a 15° steering angle during the LF transmitting mode, the grating lobe was -30 dB in amplitude compared to the main lobe (Figure 8b). In the HF mode, the -6 dB beam width at 15 mm was 0.375 mm (Figure 8c). The beam widths obtained from the acoustic mapping results (0.725 mm and 0.375 mm) were in good agreement with the simulated results (0.7 mm and 0.3 mm). With a 15° steering angle during the HF transmitting mode, a grating lobe occurred with an amplitude of -15 dB lower than the main lobe (Figure 8d). The experimentally-measured grating lobe levels of both the LF and HF configurations (-30 dB and -15 dB, respectively) were higher than those predicted in simulation (-65 dB and -45 dB, respectively). This reduced performance level is a result of cross-talk between adjacent elements which was not considered in the Field II simulation.

C. Phantom Imaging

The scan angle was set as $\pm 30^\circ$ to avoid the high grating lobes. Since the aperture size of the array was only 4 mm, the imaging area was limited. For resolution assessment, the right-most wire target pair was positioned in the middle of the S-scan. With a 30° steering angle and 25 mm depth, we expected the lateral axis to extend only 1.4 cm from the center of the S-scan. Given that the wire targets were separated by 6 mm at most, only three out of six wire pairs were visible (those located at lateral positions: 0 cm, 0.6 cm, and 1.2 cm) since the fourth target was located at a lateral position of 1.8 cm. The axial distances between wires in each of these three pairs were 0.5 mm, 1 mm, and 2 mm, respectively.

The S-scan imaging result of the L/L mode is shown in Figure 9a. Qualitatively, the first pair of wires (on the right) with a distance of 0.5 mm cannot be distinguished well; while the second pair with a vertical distance of 1 mm can be discriminated easily. As a result of the long pulse length of the low frequency signal, the axial resolution is between 0.5 mm and 1 mm.

In the L/H mode, the first pair of wires (on the right) with a distance of 0.5 mm can be barely discriminated (Figure 9b). Therefore, the axial resolution of the L/H mode is between 0.5 mm and 1 mm. The imaging result of the L/H mode is similar to the result of the L/L mode.

Figure 9c and 9d show the S-scan imaging results of the transducer array at the H/L mode and the H/H mode, respectively. For both modes, the first pair of wires with a distance of 0.5 mm are clearly identifiable. The axial resolutions of both the H/L mode and the H/H mode are much better (< 0.5 mm) than the previous modes because of the much shorter transmit pulse length.

More accurate axial and lateral imaging resolutions in different modes were further calculated by analyzing the size of the wire target responses. Raw imaging data from S-Scans were saved and processed with Matlab (MathWorks, Natick, MA.). Beam widths of wire target responses along the depth and azimuth direction were calculated separately to evaluate the axial and lateral resolutions. The axial and lateral wire target responses (with an angular position of -18° at 25 mm depth) of different modes are shown in Figure 10 (axial wire target responses) and Figure 11 (lateral wire target responses) in sequence.

For all four different imaging modes, -3 dB and -6 dB beam widths were calculated based on the wire target responses at 25 mm depth and are presented in Table III. High frequency signal (15.6 MHz) has the benefit of shorter wavelength and shorter pulse length. As expected, the H/H mode provided the highest spatial resolution of all four modes (0.36 mm in axial and 1.51 mm in lateral), while the L/L mode provided the lowest (0.56 mm in axial and 2.63 mm in lateral) because of its longer pulse length. Interestingly, the resolution of the H/L mode (0.41 mm in axial and 1.52 mm in lateral) was unexpectedly better than that of the L/H mode (0.5 mm in axial and 2.41 mm in lateral). One explanation for this could be that the transmit frequency of the H/L mode was two times higher than the transmit frequency of the L/H mode, which affected pulse length and axial resolution. On the other hand, the lateral resolution highly depends on the peak frequency component of the TX/RX echo, which in this experiment, was mainly affected by excitation frequency (Figure 12). Overall though, the results from the wire target characterization are in good agreement with the qualitative phantom imaging results.

The backscatter SNRs of all four modes were measured in the phantom to characterize the penetration depths (Figure 13). The backscatter SNR was calculated as the ratio of the high voltage (i.e. signal) to the low voltage (i.e. noise). Figure 13 shows that the penetration depths of the L/L mode and the L/H mode are larger than those of the H/H mode and the H/L mode. Because of the low-voltage limitations of the Verasonics system, the calculated backscatter SNRs are slightly underestimated.

It must be noted that the wire-target resolution results represent the combined performance of both the transducer and the chosen beamformer, which in this work was the Verasonics' pixel-based beamformer. Considering only the transducer, there were a number of factors that could have impacted resolution. First, the small aperture size resulted in a wide main lobe and poorer lateral resolution. Second, the pitch size was larger than the wavelength of the high frequency configuration, which may have resulted in larger grating lobes. Finally, cross talk between adjacent elements and an inaccurate alignment of two active layers would also induce grating lobes and improper focusing (wide main lobe), which may have impacted the SNR and resolution.

IV. Conclusion

In this paper, the design, fabrication, characterization and phantom imaging of a dual-layer bi-frequency co-linear array were presented and tested in four operating modes. To our knowledge, this is the first 1-3 composite co-linear bi-frequency array with the same aperture for both layers, making it suitable for batch fabrication.

Both electrical and acoustic element characterizations showed that elements perform consistently. This co-linear array can achieve two different resonant frequencies, 7.9 MHz with a bandwidth of 55.8 % and 19.7 MHz with a bandwidth of 31.8 %. The loop sensitivities of the LF mode and the HF mode were calculated from the pulse-echo data as -31.6 dB and -35.7 dB, respectively.

The axial resolution and lateral resolution of the L/L mode were characterized to be 0.45 mm and 2.3 mm, respectively. The L/H mode provided an axial resolution of 0.35 mm and a lateral resolution of 1.73 mm. The axial resolution derived from the H/L mode was 0.3 mm, while the lateral resolution was 1.1 mm. For the H/H mode, the axial resolution was 0.28 mm and the lateral resolution was 1 mm. As expected, the backscatter SNR of the L/L mode was better than that of the H/H mode, indicating a larger penetration depth in clinical imaging situations while the H/H mode provided better resolutions. This bi-frequency co-linear array shows potential for use in wideband fundamental imaging and harmonic/sub-harmonic imaging.

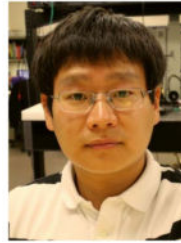
Acknowledgment

This project was supported by NIH under contract 1R41EY021392-01.

Biographies



Zhuochen Wang was born in Tianjin, China, in 1984. He received his B.S. degree in mechanical engineering from Tianjin University in 2005, and his M.S. degree in mechanical engineering from University of Akron in 2012. Zhuochen joined Dr. Xiaoning Jiang's Micro/Nano Engineering Lab at North Carolina State University in 2012, working on the design, fabrication and imaging of piezoelectric ultrasound transducers. He has a broad research interest in intravascular ultrasound (IVUS) transducer, dual frequency ultrasound transducer, transducer array and acoustic radiation force impulse imaging (ARFI) application.



Sibo Li received his B.S. degree in mechanical engineering from University of Science and technology of China in 2008, his M.S. in mechanical engineering from Stevens Institute of Technology in 2012. After that, He joined Dr. Xiaoning Jiang's group in North Carolina State University. His current research majored in transducer design and fabrication for prostate acoustic angiography, piezoelectric composite micromachined ultrasound transducers (PC-MUT) and tissue harmonic imaging.



Tomasz J. Czernuszewicz was born in Trenton, NJ, in 1985. He received his B.S. with honors degree in biomedical engineering from Marquette University in 2007. He joined Zargis Medical Corp., a startup medical device company, in 2007 where he worked as a software engineer developing computer-aided auscultation devices and telemedicine systems. In 2010 he joined the joint Department of Biomedical Engineering at the University of North Carolina - Chapel Hill and North Carolina State University and is currently working toward his Ph.D. degree. His research interests include radiation force imaging methods and vascular imaging.



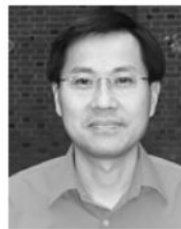
Caterina M. Gallippi is originally from Pittsburgh, PA. She earned a B.S.E. degree in electrical engineering and a certificate in engineering biology from Princeton University in 1998. She completed her Ph.D. degree in biomedical engineering at Duke University in 2003 with a focus on ultrasonic imaging. She is currently an Associate Professor in the Joint University of North Carolina at Chapel Hill, North Carolina State University department of biomedical engineering, Adjunct Associate Professor in the UNC department of radiology, and Affiliated Associate Professor in the NCSU department of electrical and computer engineering. Dr. Gallippi's research focuses on medical ultrasound technology development, particularly in the area of acoustic radiation force-based approaches to imaging the mechanical properties of tissue. Current research projects include apply her group's novel noninvasive ultrasound imaging methods to delineating the structure and composition of atherosclerotic plaques, monitoring dystrophic muscle degeneration, assess renal allograft health, and tracking subcutaneous hemorrhage.



Ruibin Liu was born in Kunming, Yunnan Province, China on July 18, 1963. He received His B.Sc. degree in electro-ceramics from The South China University of Science and Technology in 1984 and Ph.D. degree in materials engineering from The Shanghai Institute of Ceramics, Chinese Academia of Sciences in 1991. From 1991 to 1996, he was an engineer in Shanghai Institute of Ceramics. His research interest included development of pyroelectric ceramics for the application in IR detection and imaging. From 1996 to 1999, he worked as a postdoctoral in The Materials Research Laboratory of the Pennsylvania State University. His research interests there included piezoelectric actuators, single crystal thin film and electrostrictive polymers. His interests has focused on the development of ultrasound transducers especially the high frequency (>40 MHz) transducers used for high resolution imaging since 2000. He worked as a postdoctoral in Sunnybrook & Women's College Health Science Center, University of Toronto where his research interests included the fabrication of piezoelectric composite used for high frequency transducers. Then he worked as a research associate between 2004-2008 in NIH Ultrasound Transducers Resources Center, University of Southern California. His interests included fabrication of high frequency single element and array transducers for UBM and intra-cardiac vessel

imaging. In 2008, he joined the Blatek as a senior scientist. He developed and commercialized several transducers used in the catheters for intra-vascular vessel navigation and imaging.

Xuecang Geng received a B.S. degree in physics from Xi'an Jiaotong University, Xi'an, China, in 1983; an M.S. degree in acoustics from The Institute of Acoustics, Chinese Academy of Sciences, Beijing, China, in 1989; and a Ph.D. degree in material engineering from The Pennsylvania State University in 1997. From 1983 to 1986, he was an engineer at The Center of Microelectronics, Chinese Academy of Sciences, Beijing, China. His work focused on the computer-aided design of integrated circuits and the modeling of the IC process. From 1990 to 1993, as a research assistant at the ultrasonic lab of the Institute of Acoustics, he worked on nondestructive testing of materials, acoustic wave logging, and design, fabrication, and characterization of 1-3 piezocomposites for ultrasonic transducer applications. Since 1998, as a senior scientist at Blatek Inc., he has focused his effort on ultrasonic transducer design for medical and industrial applications.



Xiaoning Jiang received his B.S. in mechanical engineering from Shanghai Jiaotong University in 1990, his M.S. in mechanical engineering from Tianjin University in 1992, and his Ph.D. in precision instruments from Tsinghua University in 1997. He received Postdoctoral trainings from Nanyang Technological University and the Pennsylvania State University from 1997 to 2001. He joined Standard MEMS, Inc. as a R&D Engineer in 2001 and then worked for TRS Technologies, Inc. as a Research Scientist, Senior Scientist, Chief Scientist and Vice President for Technology before joining North Carolina State University in 2009. He is now a Professor of Mechanical and Aerospace Engineering and an Adjunct Professor of Biomedical Engineering. Dr. Jiang is the author and co-author of two book chapters, one book, 9 issued US patents, and over 60 peer reviewed journal papers and over 60 conference papers on piezoelectric composite micromachined ultrasound transducers, ultrasound for medical imaging and therapy, drug delivery, ultrasound NDT/NDE, smart materials and structures and M/NEMS. Dr. Jiang is a member of the technical program committee for IEEE Ultrasonics Symposium, UFFC representative to IEEE Nanotechnology Council, and an editorial board member for the journal Sensors.

REFERENCES

1. Crisan M, Crisan D, Sannino G, Lupsor M, Badea R, Amzica F. Ultrasonographic staging of cutaneous malignant tumors: an ultrasonographic depth index. *Arch. Dermatol. Res.* 2013; 305(4): 305–313. [PubMed: 23400334]
2. Lawrence JP. Physics and instrumentation of ultrasound. *Crit. Care Med.* 2007; 35(8):S314–22. Suppl. [PubMed: 17667455]

3. Kühl HP, Franke A, Janssens U, Merx M, Graf J, Krebs W, Reul H, Rau G, Hoffmann R, Klues HG, Hanrath P. Three-dimensional echocardiographic determination of left ventricular volumes and function by multiplane transesophageal transducer: dynamic in vitro validation and in vivo comparison with angiography and thermodilution. *J. Am. Soc. Echocardiogr.* 1998; 11(12):1113–1124. [PubMed: 9923991]
4. Belohlavek M, Tanabe K, Jakrapanichakul D, Breen JF, Seward JB. Rapid three-dimensional echocardiography clinically feasible alternative for precise and accurate measurement of left ventricular volumes. *Circulation.* 2001; 103(24):2882–2884. [PubMed: 11413074]
5. Omran H, Jung W, Rabahieh R, Wirtz P, Becher H, Illien S, Schimpf R, Lüderitz B. Imaging of thrombi and assessment of left atrial appendage function: a prospective study comparing transthoracic and transoesophageal echocardiography. *Heart.* 1999; 81(2):192–198. [PubMed: 9922358]
6. Roelandt JR, ten Cate FJ, Vletter WB, Taams MA, Bekkering L, Glastra H, Djoa KK, Weber F. Ultrasonic dynamic three-dimensional visualization of the heart with a multiplane transesophageal imaging transducer. *J. Am. Soc. Echocardiogr.* 1994; 7(3):217–229. [PubMed: 8060638]
7. Eltzschig HK, Kallmeyer IJ, Mihaljevic T, Alapati S, Shernan SK. A practical approach to a comprehensive epicardial and epiaortic echocardiographic examination. *J. Cardiothorac. Vasc. Anesth.* 2003; 17(4):422–429. [PubMed: 12968228]
8. McPherson DD, Hiratzka LF, Lamberth WC, Brandt B, Hunt M, Kieso RA, Marcus ML, Kerber RE. Delineation of the extent of coronary atherosclerosis by high-frequency epicardial echocardiography. *N. Engl. J. Med.* 1987; 316(6):304–309. [PubMed: 3807962]
9. Pandian NG, Schwartz SL, Hsu TL, Weintraub AR, Katz SE, Aronovitz M, Konstam MA, Salem DN, Kreis A. Experimental Observations on Intracavitary Imaging of Cardiac Structures with 20-MHz Ultrasound Catheters. *Echocardiography.* 1991; 8(1):127–134. [PubMed: 10149248]
10. Pandian NG, Weintraub AR, Kreis A, Schwartz SL, Konstam MA, Salem DN. Intracardiac, intravascular, two-dimensional, high-frequency ultrasound imaging of pulmonary artery and its branches in humans and animals. *Circulation.* 1990; 81(6):2007–2012. [PubMed: 2188760]
11. de Jong N, Frinking PJ, Bouakaz A, ten Cate FJ. Detection procedures of ultrasound contrast agents. *Ultrasonics.* 2000; 38(1):87–92. [PubMed: 10829635]
12. Frinking PJ, Bouakaz A, Kirkhorn J, ten Cate FJ, de Jong N. Ultrasound contrast imaging: current and new potential methods. *Ultrasound Med. Biol.* 2000; 26(6):965–975. [PubMed: 10996696]
13. Smith WA, Auld BA. Modeling 1-3 composite piezoelectrics: thickness-mode oscillations. *IEEE Trans. Ultrason. Ferroelectr. Freq. Control.* 1991; 38(1):40–47. [PubMed: 18267555]
14. Jiang X, Yuan JR, Snook K, Rehrig PW, Shrout TR, Hackenberger Wesley S, Cheng A, Cao P, Lavalelle G, Geng X. Microfabrication of Piezoelectric Composite Ultrasound Transducers (PC-MUT). *IEEE Ultrason. Symp.* 2006:922–925.
15. Shen ZY, Li JF, Chen R, Zhou Q, Shung KK. Microscale 1-3-Type (Na, K) NbO₃-Based Pb-Free Piezocomposites for High-Frequency Ultrasonic Transducer Applications. *J. Am. Ceram. Soc.* 2011; 94(5):1346–1349. [PubMed: 21637726]
16. Li S, Jiang X, Tian J, Han P. Development of dual-layer micromachined composite transducers for broadband ultrasound imaging. *IEEE Int. Ultrason. Symp.* 2014:667–670.
17. Ritter T, Geng X, Kirk Shung K, Lopath PD, Park SE, Shrout TR. Single crystal PZN/PT-polymer composites for ultrasound transducer applications. *IEEE Trans. Ultrason. Ferroelectr. Freq. Control.* 2000; 47(4):792–800. [PubMed: 18238611]
18. Jiang X, Snook K, Walker T, Portune A, Haber R, Geng X, Welter J, Hackenberger WS. Single crystal piezoelectric composite transducers for ultrasound NDE applications. *Proc. SPIE.* 2008:573–576.
19. Oakley CG, Zipparo MJ. Single crystal piezoelectrics: a revolutionary development for transducers. *IEEE Ultrason. Symp.* 2000; 2:1157–1167.
20. Brown JA, Foster FS, Needles A, Cherin E, Lockwood GR. Fabrication and performance of a 40-MHz linear array based on a 1-3 composite with geometric elevation focusing. *IEEE Trans. Ultrason. Ferroelectr. Freq. Control.* 2007; 54(9):1888–1894. [PubMed: 17941395]

21. de Fraguier S, Gelly JF, Wolnerman L, Lannuzel O. A novel acoustic design for dual frequency transducers resulting in separate bandpass for color flow mapping (CFM). *IEEE Ultrason. Symp.* 1990:799–803.
22. Saitoh S, Izumi M, Mine Y. A dual frequency ultrasonic probe for medical applications. *IEEE Trans. Ultrason. Ferroelectr. Freq. Control.* 1995; 42(2):294–300.
23. Hossack JA, Mauchamp P, Ratsimandresy L. A high bandwidth transducer optimized for harmonic imaging. *IEEE Ultrason. Symp.* 2000; 2:1021–1024.
24. Wang Z, Li S, Jiang X, Liu R, Geng X. Design, fabrication and characterization of a bi-frequency co-linear array (7.5MHz/15MHz). *IEEE Int. Ultrason. Symp.* 2013:504–507.
25. Mann JA, Walker WF. A constrained adaptive beamformer for medical ultrasound: Initial results. *IEEE Ultrason. Symp.* 2002; 2:1807–1810.
26. Chen Y, Nguyen M, Yen JT. A 5-MHz cylindrical dual-layer transducer array for 3-D transrectal ultrasound imaging. *Ultrason. Imaging.* 2012; 34(3):181–195. [PubMed: 22972914]
27. Azuma T, Ogihara M, Kubota J, Sasaki A, Umemura S, Furuhashi H. Dual-frequency ultrasound imaging and therapeutic bilaminar array using frequency selective isolation layer. *IEEE Trans. Ultrason. Ferroelectr. Freq. Control.* 2010; 57:1211–1224. [PubMed: 20442033]
28. Souquet J, Defranould P, Desbois J. Design of low-loss wide-band ultrasonic transducers for noninvasive medical application. *IEEE Trans. Sonics. Ultrason.* 1979; 26(2):75–80.
29. Ma J, Jiang X, Martin KH, Dayton PA. Small aperture, dual frequency ultrasound transducers for intravascular contrast imaging. *IEEE Int. Ultrason. Symp.* 2013:769–772.
30. Krimholtz R, Leedom DA, Mattaei GL. New equivalent circuits for elementary piezoelectric transducers. *Electron. Lett.* 1970; 41:398–399.
31. Ma J, Martin KH, Dayton PA, Jiang X. A preliminary engineering design of intravascular dual-frequency transducers for contrast-enhanced acoustic angiography and molecular imaging. *IEEE Trans. Ultrason. Ferroelectr. Freq. Control.* 2014; 61(5):870–880. [PubMed: 24801226]
32. Jensen JA. Field: A Program for Simulating Ultrasound Systems. *Med. Biol. Eng. Comput.* 1996; 34(1):351–353. suppl. 1. [PubMed: 8945858]
33. Jensen JA, Svendsen NB. Calculation of pressure fields from arbitrarily shaped, apodized, and excited ultrasound transducers. *IEEE Trans. Ultrason. Ferroelectr. Freq. Control.* 1992; 39:262–267. [PubMed: 18263145]
34. Wang Z, Li S, Jiang X, Liu R, Geng X. Design and phantom testing of a bi-frequency co-linear array. *IEEE Int. Ultrason. Symp.* 2014:2108–2111.
35. Wang Z, Li S, Liu R, Geng X, Jiang X. A Bi-Frequency Co-Linear Array Transducer for Biomedical Ultrasound Imaging. *ASME Int. Mech. Eng. Congress. Expo.* 2014:V003T03A085.
36. Üstüner, KF.; Holley, GL. Ultrasound imaging system performance assessment; presented at AAPM Annu. Meeting; 2003.

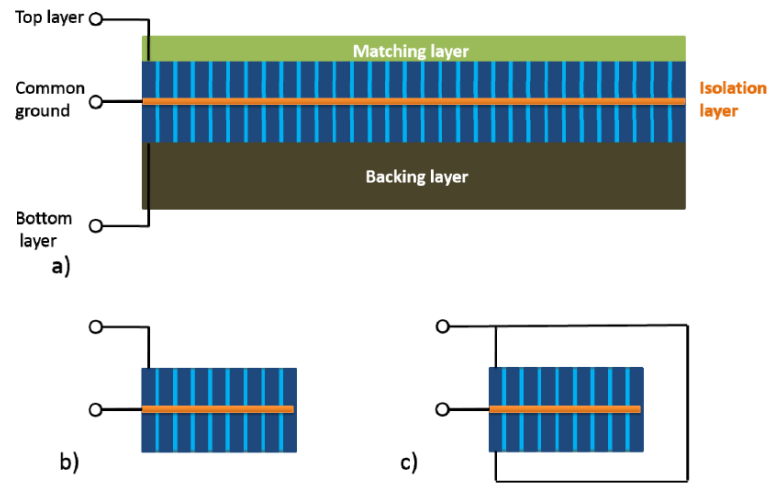


Fig. 1.

- a) Schematic view of the 32-element co-linear array. b) HF mode (only top layer is active).
 c) LF mode (both layers activated in parallel).

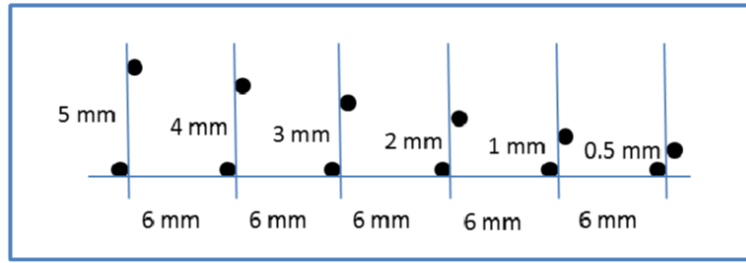


Fig. 2.
Sketch of the commercial wire phantom.

Author Manuscript

Author Manuscript

Author Manuscript

Author Manuscript

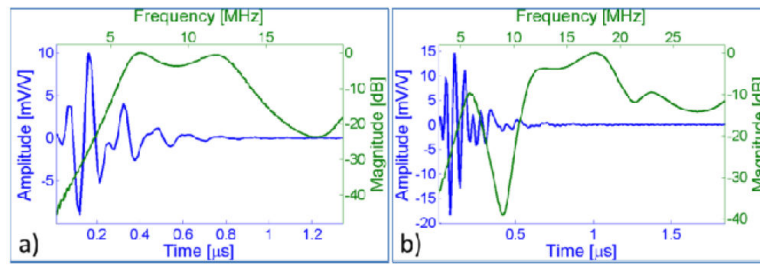


Fig. 3. Simulation of pulse-echo responses based on the KLM model. a) LF mode. b) HF mode.

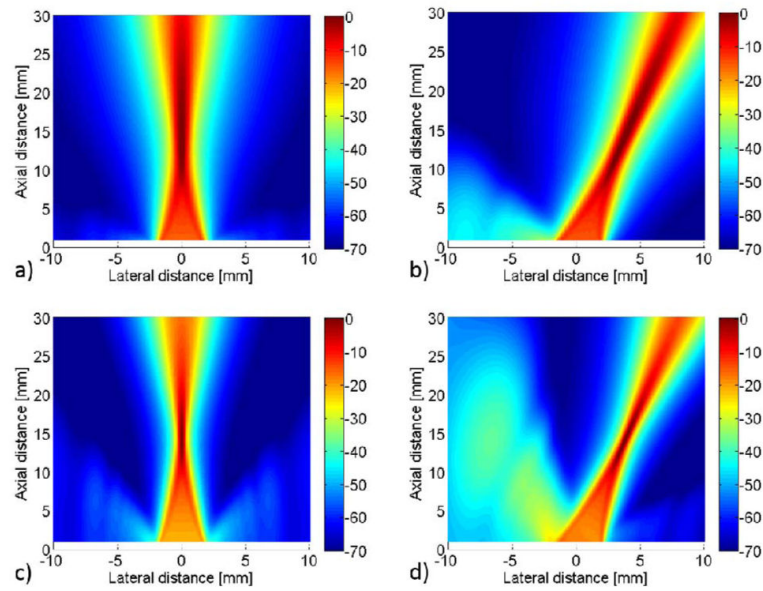


Fig. 4.

Simulation of transducer beam profiles using the Field II program. All beam profiles were simulated with a 15 mm focus. a) Beam profile of the LF transmitting mode without any steering. b) Beam profile of the LF transmitting mode with a 15° steering angle. c) Beam profile of the HF mode without any steering. d) Beam profile of the HF mode and with a 15° steering angle. The color bar represents normalized magnitude in dB.

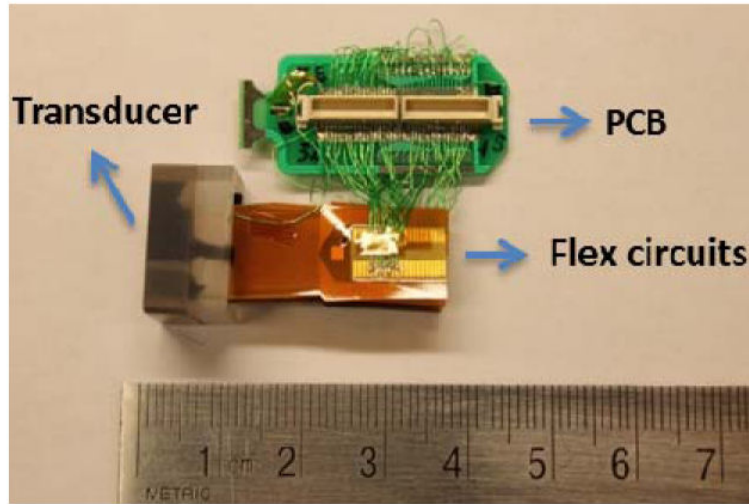


Fig. 5.
Photograph of the co-linear array.

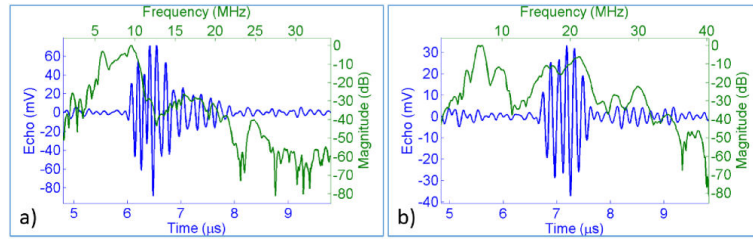


Fig. 6. Experimentally-measured pulse-echo results. a) LF mode. b) HF mode.

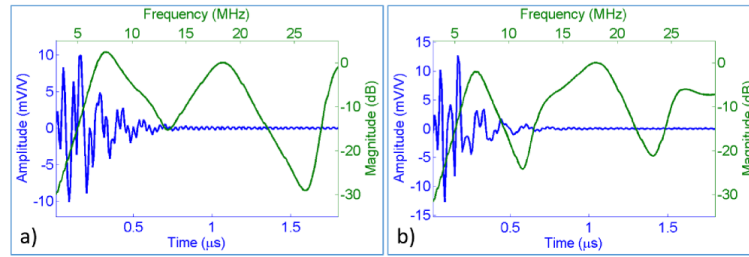


Fig. 7.

Pulse-echo response simulations of the high frequency layer by using the KLM model. The frequency domain has been normalized to the high frequency component (the second peak).

a) -6 dB bandwidth of the HF mode without isolation layer is 24%. b) -6 dB bandwidth of the HF mode with a 2 μm isolation layer is 30%.

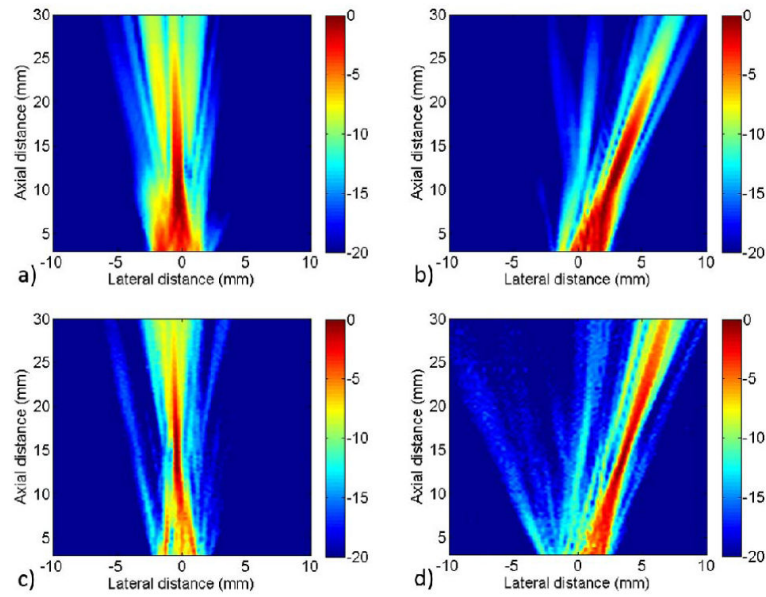


Fig. 8. Beam profile mapping of the 32-element co-linear array. a) LF transmitting mode with no beam steering, focused at 15 mm. b) LF transmitting mode with 15° steering angle, focused at 15 mm. c) HF transmitting mode with no beam steering, focused at 15 mm. d) HF transmitting mode with 15° steering angle, focused at 15 mm. The color bar indicates normalized magnitude in units of dB.

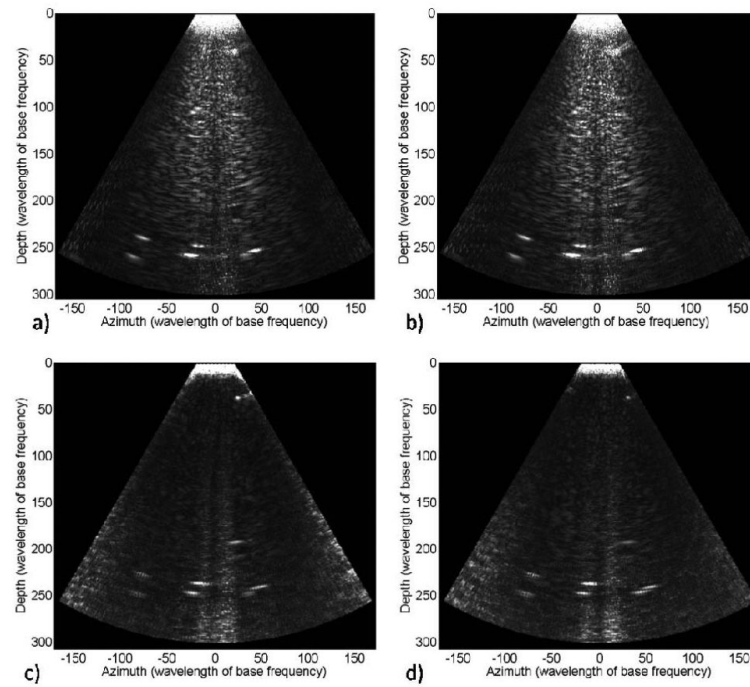


Fig. 9. Resolution test with a focal depth of 250 wavelengths (25 mm). a) L/L mode. b) L/H mode. c) H/L mode. d) H/H mode.

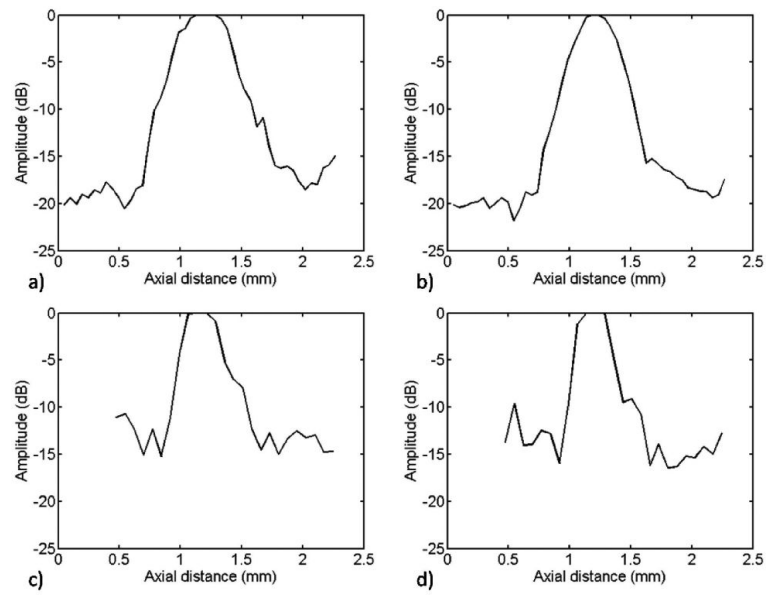


Fig. 10. Axial wire target responses. a) L/L mode. b) L/H mode. c) H/L mode. d) H/H mode.

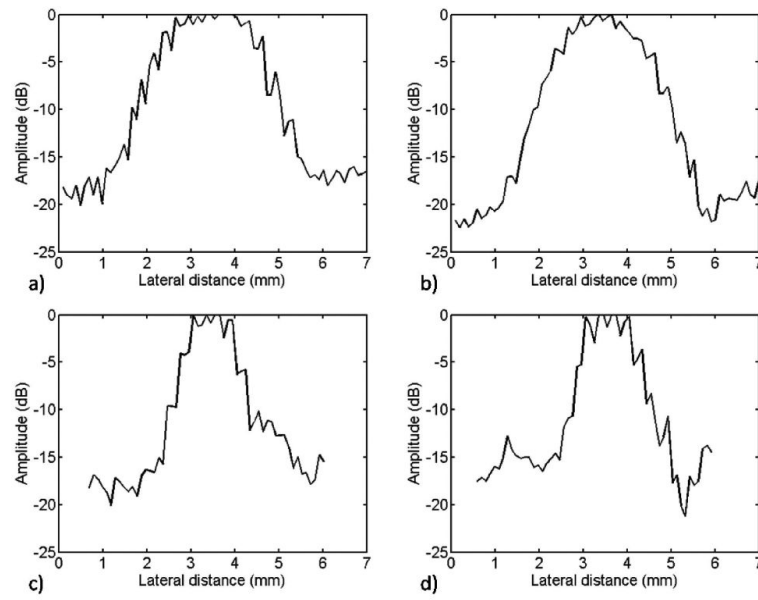


Fig. 11. Lateral wire target responses. a) L/L mode. b) L/H mode. c) H/L mode. d) H/H mode.

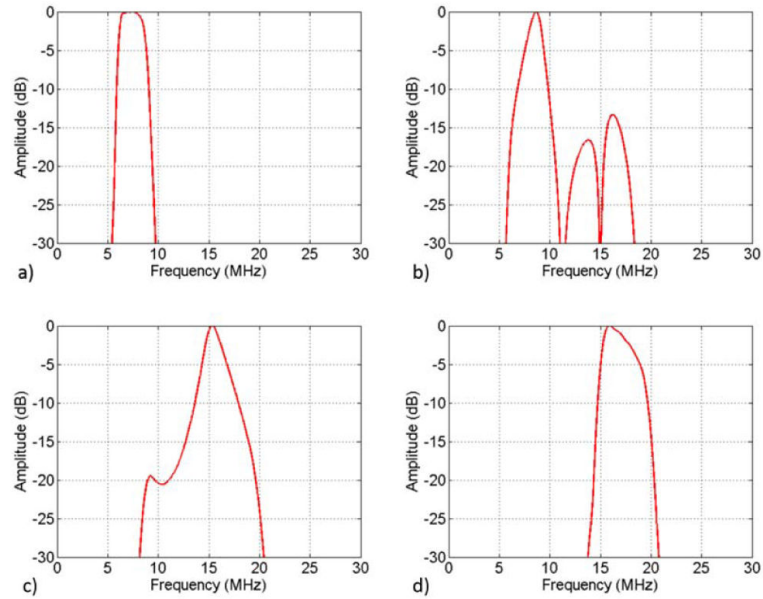


Fig. 12.

Frequency plots of pulse/echo simulations with a 2-cycle sinusoid excitation for all four modes. The low and high frequency layers were modeled as bandpass filters with center frequency and bandwidth matched to our experimental measurements. The frequency response of the echo was determined by the Fourier transform of the filtered 2-cycle excitation waveform. a) L/L mode only has a low frequency component. b) L/H mode is dominated by the low frequency component. c) H/L mode is dominated by the high frequency component. d) H/H mode only has a high frequency component. These simulation results show that the resolutions of the reported bi-frequency transducer array are highly dependent upon the values of the excitation frequencies.

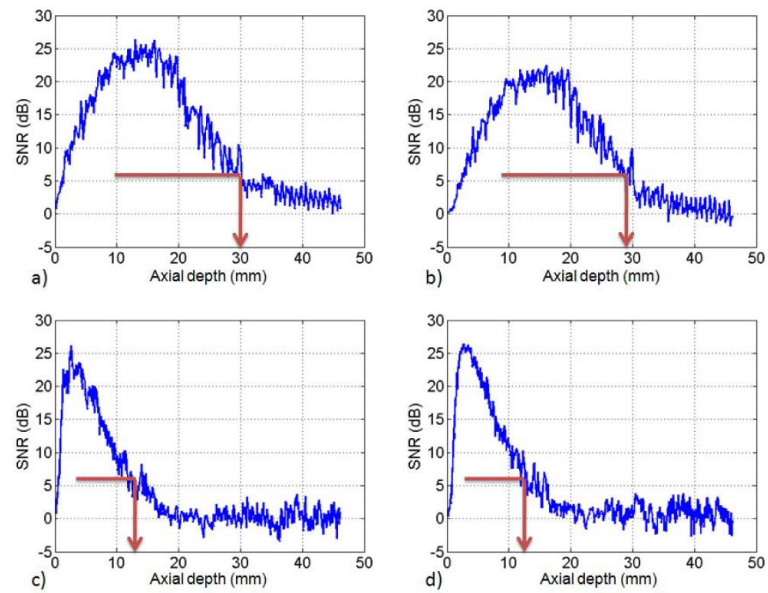


Fig. 13.

The backscatter SNR characterization in a phantom by using the Verasonics system. a) L/L mode. b) L/H mode. c) H/L mode. d) H/H mode. Red arrows indicate the depth at which the SNR drops below -6 dB. The results show that the L/L mode has a larger penetration depth than that of the H/H mode.

TABLE I

DESIGN PARAMETERS OF THE DUAL-LAYER STRUCTURE

	Backing Layer	#1 Active Layer	Isolation Layer	#2 Active Layer	Matching Layer
Impedance (MRayl)	4.48	18.2	2.85	18.2	5.2
Thickness (μm)	3000	100	10	100	55
Attenuation (dB/cm·MHz)	8	0.3	4.5	0.3	0.3

Author Manuscript

Author Manuscript

Author Manuscript

Author Manuscript

TABLE II**B**EAM **P**ROFILE **S**IMULATION **R**ESULTS

	LF mode			HF mode		
	0.7 mm			0.3 mm		
-6 dB beam width at 15mm						
Steering angle	15°	30°	40°	15°	30°	40°
Grating lobe (dB)	-65	-55	-41	-45	-23	-16

Author Manuscript

Author Manuscript

Author Manuscript

Author Manuscript

TABLE III

AXIAL AND LATERAL BEAM WIDTH MEASUREMENT RESULTS

	-3 dB wire target response (beam width)		-6 dB wire target response (beam width)	
	Axial	Lateral	Axial	Lateral
L/L mode	0.45 mm	2.3 mm	0.56 mm	2.63 mm
L/H mode	0.35 mm	1.73 mm	0.5 mm	2.41 mm
H/L mode	0.3 mm	1.1 mm	0.41 mm	1.52 mm
H/H mode	0.28 mm	1 mm	0.36 mm	1.51 mm

Author Manuscript

Author Manuscript

Author Manuscript

Author Manuscript